Experimental Simulations of Sulfide Formation in the Solar Nebula

Dante S. Lauretta; Katharina Lodders; Bruce Fegley Jr.

Science, New Series, Volume 277, Issue 5324 (Jul. 18, 1997), 358-360.

Stable URL:
http://links.jstor.org/sici?sici=0036-8075%2819970718%293%3A277%3A5324%3C358%3AESOSFI%3E2.0.CO%3B2-%23

umn densities of about 6×10^{14} cm^{-2} and 3.6×10^{15} cm^{-2} are obtained for assumed neutral atmosphere scale heights of 20 and 120 km, respectively. Even the larger column density, if reduced by the factor of 5 corresponding to additional electron impact ionization, brings the required column density below the value set by Hall *et al.* (6). It should also be pointed out that these column densities do lead to an optical depth of less than unity, which was assumed at the beginning of this discussion. It is now appropriate to address the validity of the assumption of chemical equilibrium conditions. The chemical time constant near the surface (~500 s), given the observed scale height, is significantly smaller than the diffusive time constant (~10^4 s); thus, the assumption is a good one.

The near-surface atmospheric densities and temperatures that were found to be consistent with the ionospheric observations, namely a number density of ~10^8 cm^{-3} and a temperature of ~340 to 600 K, correspond to a surface pressure of 0.01 nbar. This value is comparable to about the limit set by the Voyager UV spectrometer for Ganymede (*16*), but no comparable limits are available for Europa.

A very unlikely scenario would lead to a density requirement that is significantly lower than any discussed here so far. This is the case of an atmosphere that consists solely of atomic hydrogen or oxygen, with no molecular species being present. The required atmospheric density is very different in this case, because the loss of atomic ions by either radiative recombination, corresponding to a lifetime of about 10^7 s, or diffusion to the surface, with a lifetime of about 10^6 s, are both very slow processes. In this scenario, transport processes related to Europa's interaction with Jupiter's magnetosphere are likely to be most important.

Finally, it should be pointed out that the external magnetospheric thermal plasma and magnetic pressures on Europa's ionosphere are about 2×10^{-8} and 2×10^{-7} Nm^{-2}, respectively. Even if the electron and ion temperatures are allowed to be four times greater than the neutral gas temperature, the peak ionospheric thermal plasma pressure, calculated with the measured peak electron density, is still significantly less than the external one. This means that the ionosphere will be strongly magnetized and coupled to the magnetosphere.

REFERENCES AND NOTES

1. Radio occultations, in which a spacecraft appears to go behind a planetary body as viewed from Earth, allow the spacecraft-Earth radio link to traverse the ionosphere and atmosphere of the occulting body. Interpretation of the effects on the phase and amplitude of the signal received on Earth of refraction and defocusing in the planetary atmosphere and ionosphere allows one to infer the electron density structure in the ionosphere and the temperature-pressure profiles and absorption characteristics of the neutral atmosphere. This technique has been used with much success to measure the characteristics of the ionospheres and atmospheres of Venus, Mars, Jupiter, Saturn, Uranus, and Neptune, as well as Saturn's satellite Titan, Neptune's Triton, and Jupiter's Io and now Europa (*12*).
2. A. J. Kliore, D. L. Cain, G. Fjeldbo, B. L. Seidel, S. I. Rasool, *Science* **183**, 323 (1974).
3. R. E. Johnson, *Energetic Charged-Particle Interactions with Atmospheres and Surfaces* (Springer Verlag, Berlin, 1990).
4. W. H. Ip, *Icarus* **120**, 317 (1996).
5. F. M. Wu, D. L. Judge, R. W. Carlson, *Astrophys. J.* **325**, 325 (1978).
6. D. T. Hall, D. F. Strobel, P. D. Feldman, M. A. McGrath, H. A.Weaver, *Nature* **373**, 677 (1995).
7. C. Barth *et al.*, *Geophys. Res Lett.*, in press; C. Barth, personal communication.
8. H. T. Howard *et al.*, *Space. Sci. Rev.* **60**, 565 (1992).
9. The PLO is used to steer the center frequency of the receiver bandwidth in accordance with a predicted function based on the spacecraft trajectory.
10. G. Fjeldbo, A. J. Kliore, V. R. Eshleman, *Astron. J.* **76**, 123 (1971).
11. A. J. Kliore, in *NASA TM X-62,150*, L. Colin, Ed. (NASA/Ames Research Center, Mountain View, CA, 1972).
12. G. F. Lindal, *Astron. J.* **103**, 967 (1992).
13. M. R. Torr and D. G. Torr, *J. Geophys. Res.* **90**, 6675 (1985).
14. R. Schreier, A. Eviatar, V. M. Vasyliunas, J. D. Richardson, *ibid.* **98**, 21231 (1993).
15. W. M. Calvin, R. N. Clark, R. H. Brown, J. R. Spencer, *ibid.* **100**, 19041 (1995).
16. L. Broadfoot *et al.*, *Science* **204**, 979 (1979); S. Kumar and D. M. Hunten, in *Satellites of Jupiter*, D. Morrison, Ed. (Univ. of Arizona Press, Tucson, AZ, 1982), pp. 782–806.

17. We wish to acknowledge the contributions of the staff of the Galileo Project, who have carried out a highly successful mission under difficult circumstances; the Galileo Navigation team, with W. E. Kirhofer and J. Johannesen, without whose precise orbits this work would not have been possible; and the personnel of the Jet Propulsion Laboratory Multimission Radio Science team, especially S. Asmar, R. Herrera, D. Chong, P. Eshe, P. Priest, J. Caetta, T. Rebold, and S. Abbate, who planned and successfully executed the data acquisition process. Special thanks are due to J. Twicken and P. Schinder for their assistance in data analysis at Stanford and Goddard Space Flight Center, and to D. M. Hunten, W. H. Ip, and two anonymous referees for helpful suggestions and comments. This work was supported by NASA contracts and grants.

28 April 1997; accepted 17 June 1997

Experimental Simulations of Sulfide Formation in the Solar Nebula

Dante S. Lauretta,* Katharina Lodders, Bruce Fegley Jr.

Sulfurization of meteoritic metal in H_2S-H_2 gas produced three different sulfides: monosulfide solid solution [$(Fe,Ni)_{1-x}S$], pentlandite [$(Fe,Ni)_{9-x}S_8$], and a phosphorus-rich sulfide. The composition of the remnant metal was unchanged. These results are contrary to theoretical predictions that sulfide formation in the solar nebula produced troilite (FeS) and enriched the remaining metal in nickel. The experimental sulfides are chemically and morphologically similar to sulfide grains in the matrix of the Alais (class CI) carbonaceous chondrite, suggesting that these meteoritic sulfides may be condensates from the solar nebula.

Chondrites are the most primitive meteorites and may contain condensates that could serve as probes of the solar nebula environment. Unfortunately, even the most primitive meteorites experienced some degree of secondary processing—such as aqueous alteration, thermal metamorphism, or impact shock—that transformed nebular condensates into secondary phases. Therefore, criteria to distinguish pristine nebular condensates from secondary alteration products in chondrites are required. Experimental simulations of the gas-solid reactions that formed nebular minerals are one method to determine such criteria.

Planetary Chemistry Laboratory, Department of Earth and Planetary Sciences, Campus Box 1169, Washington University, One Brookings Drive, St. Louis, MO 63130–4899, USA.

*To whom correspondence should be addressed. E-mail: lauretta@wunder.wustl.edu

Sulfide minerals are ubiquitous in chondrites. The most common sulfides in carbonaceous chondrites are pyrrhotite ($Fe_{1-x}S$) and pentlandite [$(Fe,Ni)_{9-x}S_8$] (*1*). Stoichiometric pyrrhotite is troilite (FeS), and Ni-bearing pyrrhotites are members of the monosulfide solid solution [mss, $(Fe,Ni)_{1-x}S$]. In addition, P-bearing sulfides were recently found in CM chondrites (*2*, *3*). Because the characteristics of nebular sulfides were poorly understood, we experimentally simulated their formation in the solar nebula to determine the resulting mineralogy, morphology, and composition (*4*). By characterizing nebular sulfides in this manner, we can determine which, if any, of the sulfides in carbonaceous chondrites are unaltered nebular condensates.

We formed an experimental metal-sulfide assemblage by heating a piece of the Canyon Diablo iron meteorite for 30 days

at 340°C in 50 parts per million (ppm) of H_2S in H_2. The morphology of this sample (Fig. 1) is typical of sulfides formed by the corrosion of Fe-based alloys (*5*, *6*). Small grains of Ni- and P-rich sulfide form a thin, porous layer above the remnant metal. The outer sulfide layer is composed of crystals formed from compact grains of mss uniformly orientated along their crystallographic *a* axes. Pentlandite inclusions are dispersed throughout the outer layer. The Ni content of the outer sulfide layer increases from its bottom edge toward its top. Despite the variation in the Ni concentration of the sulfide layer, the bulk Fe/Ni ratio in the remaining metal is similar to that in the newly formed sulfide at all temperatures studied (285°, 340°, and 370°C). In contrast, condensation calculations predict the formation of Ni-free troilite in the solar nebula (*5*, *7*) through the reaction (8)

$$\text{kamacite } (\alpha) + H_2S\ (g) = \text{kamacite } (\alpha) + \text{taenite } (\gamma) + FeS + H_2\ (g) \quad (1)$$

Metallurgical studies of binary-alloy corrosion show that thermodynamics and diffusion-controlled kinetics influence the cation distribution between metal and sulfide (*9*). These relationships are illustrated by a diffusion path that traces the compositional variation of a metal-sulfide assemblage on a ternary phase diagram. The diffusion path (*10*) for an experimental metal-sulfide assemblage (Fig. 2) was determined with an electron microprobe traverse starting at the unreacted metal core, proceeding through the sulfide layer, and ending at the sulfurizing atmosphere.

The system starts out as a solar composition alloy (point a: 94 weight % Fe, 6 weight % Ni). The sulfide in equilibrium with this alloy is troilite containing very little Ni (~0.06 weight %) (*11*). Thus, troilite is the first sulfide to form. Transfer of Fe atoms from the metal to the sulfide enriches the metal in Ni, and the Ni composition of the FeNi alloy at the interface increases toward point b (58 weight % Fe, 42 weight % Ni) (*12*). Thus, sulfurization of FeNi metal is predicted to produce a thin region of Ni-enriched metal. The width of this region is controlled by the diffusion rate of Fe and Ni in the metal and remains constant throughout the course of the reaction (*9*). The amount of Ni soluble in sulfide increases in proportion to the Ni content of the metal at the interface. The sulfide in equilibrium with the Ni-rich metal (point b) at 370°C contains ~1 weight % Ni (point c) and has an Fe/Ni ratio less than that of the initial metal (*11*). To form this Ni-bearing sulfide, Fe and Ni atoms diffuse through the sulfide layer to the sulfide-gas interface. In the sulfide, Ni diffuses faster than Fe, creating a Ni concentration gradient (between points c and d) (*13*). As a result, the outer portion of the sulfide layer has higher concentrations of Ni than the starting metal. However, the bulk Fe/Ni ratio is similar in the metal and sulfide. The rate of cation diffusion in the sulfide is most rapid along the *a* axis of the hexagonal unit cell (*14*); thus, cation transport is most rapid in crystals with their *a* axes perpendicular to the metal surface, and these crystals quickly outgrow other sulfide crystals. This preferred direction of growth results in a uniform orientation of the outer crystals. Eventually, the Ni concentration at the outer edge of the sulfide exceeds the solubility limit, and pentlandite crystals exsolve from the mss layer (points d and e). It is also possible that pentlandite exsolves from the mss as it cools in the solar nebula; this occurs when metal is sulfurized above 610°C, where pentlandite is unstable (*15*). Such a sulfide would still be a product of a gas-solid reaction in the solar nebula.

The sulfide formation process also influences the overall layer morphology. The outward diffusion of Fe and Ni causes the metal surface to retreat from the metal-sulfide interface. The increase in molar volume associated with sulfide formation imposes stresses that force the sulfide layer to deform plastically into the newly created void and reestablish contact with the metal surface. The sulfide layer fractures when its plastic deformation limit is reached, allowing gas to penetrate directly to the metal surface and form a second, inner sulfide layer.

In our experiments, we did not observe

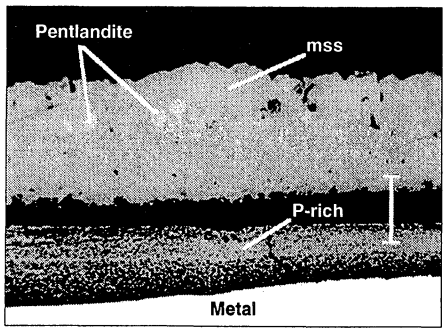

Fig. 1. An optical reflected light image of an experimental sample reacted at 340°C in 50 ppm of H_2S in H_2 for 30 days. The remnant metal core (white) is at the bottom. The black material is epoxy-filled void space. The sulfide layer is composed of three phases: a P-rich sulfide (inner fine-grained layer), the monosulfide solid solution (dark gray phase in outer layer), and pentlandite (light gray phase in outer layer). Scale bar = 32 μm.

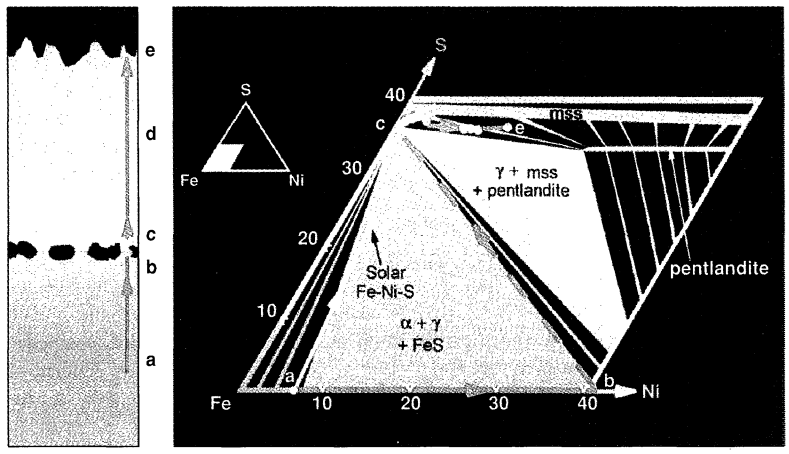

Fig. 2. A cartoon of a sulfide layer (**left**) and the Fe-rich portion of the Fe-Ni-S isothermal ternary phase diagram at 400°C (**right**) (*15*). The reaction path proposed by Kerridge *et al.* (*17*) is shown as the white line on the phase diagram. Their predicted final assemblage is a kamacite (α)–taenite (γ) metal core surrounded by a rim of troilite (FeS). The direction of the electron microprobe traverse across the experimental assemblage is indicated by the red arrows on the cartoon. The black blebs indicate the porous inner layer, and the yellow blebs symbolize pentlandite grains in the outer layer. The shading corresponds to chemical variations in the assemblage similar to the shading on the ternary diagram. The results of the traverse are plotted as green dots on the phase diagram. The red curves connecting the microprobe data trace the diffusion path followed during the sulfurization reaction. The dashed line b-c indicates equilibrium between metal (point b) and sulfide (point c) compositions at the interface and represents no spatial extent. A Ni- and P-rich phase ultimately consumes the Ni-rich metal indicated by point b. The final experimental assemblage contains a kamacite core surrounded by sulfide rims composed of P-rich sulfides, the monosulfide solid solution (mss), and pentlandite.

the Ni-rich metal (point b) predicted to form during binary-alloy sulfurization (9). Instead, we found inner sulfide layers enriched in Ni and P (16). Because we used P-bearing FeNi alloys, the enrichment of Ni in the metal was accompanied by an enrichment in P. Eventually, the Ni and P concentrations at the metal-sulfide interface reached a level where the observed Ni-rich, P-bearing sulfide phase became stable. Diffusion of Ni and P in the inner layer created a second concentration gradient with both Ni and P decreasing away from the metal. The formation of the inner sulfide layer consumed the Ni-rich metal. Thus, there was no increase in the Ni content of the metal resulting from sulfurization.

The assemblage resulting from sulfurization of meteoritic metal was a kamacite core surrounded by a fine-grained, porous, Ni- and P-rich inner sulfide layer and a blocky, uniformly oriented, outer mss layer with pentlandite inclusions. The metal and sulfide layers were typically separated from each other by large gaps. These gaps allowed the sulfide layers to easily detach from the metal during collisions in the solar nebula. Thus, the metal and the two types of sulfide layers are likely to be dispersed throughout the matrices of primitive meteorites.

Kerridge *et al.* (17) used the low-temperature Fe-Ni-S phase diagram to predict the path of reaction 1 under solar nebula conditions. They assumed that sulfurization proceeds as a linear addition of S to Fe-Ni metal. The reaction path (Fig. 2) starts at the composition of a solar FeNi alloy (94 weight % Fe, 6 weight % Ni), moves directly toward the S apex, and stops at the point corresponding to the solar abundance of Fe, Ni, and S (74 weight % Fe, 4 weight % Ni, 22 weight % S) (18, 19) in the α-γ-FeS field. Thus, Kerridge *et al.* (17) predict that sulfurization of an FeNi alloy produces a troilite rim around a kamacite-taenite metal core. However, the assumption of a linear reaction path does not take into account reaction kinetics, such as diffusion in the sulfide layer or in the metal alloy.

Measurements of ^{129}Xe excesses in CI chondrite sulfides suggest a solar nebula origin (20). Kerridge *et al.* (17) performed chemical and isotopic analyses of sulfides from the Orgueil, Ivuna, and Alais CI chondrites. The dominant sulfide phase in all three CI chondrites is mss containing 0.70 to 1.32 weight % Ni. In addition, some of the Alais sulfides have inclusions of pentlandite containing ~34 weight % Ni. Kerridge *et al.* (17) concluded that the Alais sulfides could not be nebular products formed under equilibrium conditions, based on their interpretation of the theoretical reaction path for FeNi alloy sulfurization. Our experiments provide a better means of determining the composition and morphology of sulfides formed by gas-solid reaction in the nebula. The composition and morphology of the Alais sulfides are similar to those in our experimental samples, implying that they may be nebular condensates.

Nazarov *et al.* (2) performed a survey of sulfide minerals in Mighei (CM) and found pyrrhotite and pentlandite to be the dominant sulfide phases. They also found several P-rich accessory sulfide phases. Further investigations revealed that these P-rich phases are ubiquitous in CM chondrites (3). The origin of the P-bearing sulfides has not been determined. Current petrographic evidence is ambiguous, suggesting either condensation in the solar nebula (2) or formation during aqueous alteration (3). The chondritic P-rich sulfides are chemically and morphologically similar to the inner sulfide layers of our experiments, pointing to a nebular origin (16).

The occurrence of sulfide phases with old ^{129}Xe ages in primitive chondrites that have compositions and morphologies similar to those produced in our condensation experiments suggests that they may be condensates from the solar nebula. It is unclear whether these phases can be produced by aqueous alteration on the meteorite parent body. Pentlandite formed by aqueous alteration or terrestrial weathering of troilite would occur along the edges of the altered sulfide grain. Such secondary alteration products are recognized in meteorites (21). Secondary alteration should not produce pentlandite inclusions within mss grains. Sulfides with this morphology most likely formed by sulfurization of FeNi alloys and are good candidates for nebular products. Experimental analogs of metal-sulfide assemblages resulting from aqueous alteration are needed to resolve these issues.

REFERENCES AND NOTES

1. P. Ramdohr, *J. Geophys. Res.* **68**, 2011 (1963); R. E. Folinsbee, J. A. V. Douglas, J. A. Maxwell, *Geochim. Cosmochim. Acta* **31**, 1625 (1967); J. F. Kerridge, J. D. MacDougall, J. Carlson, *Earth Planet. Sci. Lett.* **43**, 1 (1979); G. R. Huss, K. Keil, G. J. Taylor, *Geochim. Cosmochim. Acta* **45**, 33 (1981).
2. M. A. Nazarov, F. Brandstaetter, G. Kurat, *Lunar Planet. Sci.* **XXVII**, 939 (1996).
3. B. Devouard and P. R. Buseck, *Meteorit. Planet. Sci.*, in preparation.
4. A solar-composition metal contains 93.8 weight % Fe, 5.4 weight % Ni, 0.3 weight % Co, and 0.6 weight % P (18). A solar-composition gas is composed mainly of H_2 and contains 33 ppm of H_2S (19). For these compositions, sulfide minerals are stable below the pressure-independent temperature of 437°C (5). Experiments were performed on polished, inclusion-free slabs of the Canyon Diablo iron meteorite (92.8 weight % Fe, 6.5 weight % Ni, 0.5 weight % Co, and 0.2 weight % P) heated at 285°, 340°, or 370°C for up to 1 month in 50 ppm of H_2S in H_2 at ambient atmospheric pressure.
5. D. S. Lauretta, D. T. Kremser, B. Fegley Jr., *Icarus* **122**, 288 (1996).
6. ———, *Proc. NIPR Symp. on Antarctic Meteorites* **9**, 97 (1996); D. S. Lauretta, B. Fegley Jr., K. Lodders, D. T. Kremser, *ibid.*, p. 111.
7. H. C. Urey, *The Planets* (Yale Univ. Press, New Haven, CT, 1952); J. W. Larimer, *Geochim. Cosmochim. Acta* **31**, 1215 (1967); J. S. Lewis, *Earth Planet. Sci. Lett.* **15**, 286 (1972).
8. Iron-nickel alloys containing less than 7.5% Ni are kamacite (α). Iron metal with more than 25% Ni is taenite (γ). Intermediate compositions are in the α-γ two-phase field.
9. See the review by B. D. Bastow, G. C. Wood, D. P. Whittle, *Corros. Sci.* **25**, 253 (1985), and references therein.
10. The conventions for plotting the diffusion path on isothermal ternary phase diagrams are outlined by J. B. Clark, *Trans. AIME* **227**, 1250 (1963).
11. The Ni content of the sulfide in equilibrium with metal depends on temperature and metal composition. This relation is discussed in D. S. Lauretta, D. T. Kremser, B. Fegley Jr., *Lunar Planet. Sci.* **XXVI**, 831 (1995).
12. The Fe and Ni diffusion coefficients in 95 weight % Fe–5 weight % Ni metal at 400°C are $\sim 10^{-22}$ and $\sim 10^{-23}$ cm^2 s^{-1}, respectively (22). This slow diffusion prevents the metal from homogenizing. As a result, relatively Ni-rich sulfides are in equilibrium with the Ni-rich metal. The rate of sulfide formation is limited by the rate of cation diffusion through the sulfide layer (14). The Fe diffusion coefficient in pyrrhotite at 400°C is $\sim 10^{-11}$ cm^2 s^{-1} (14), and the Ni diffusion coefficient in the mss at 400°C is $\sim 10^{-10}$ cm^2 s^{-1} (13). Thus, sulfide formation is ~10 orders of magnitude faster than cation diffusion in the metal. This difference in diffusion rate is the main reason that Ni-bearing sulfides form.
13. J. P. Orchard and D. J. Young, *J. Electrochem. Soc.* **136**, 545 (1989); *Oxid. Met.* **31**, 105 (1989); T. Narita and K. Nishida, *Denki Kagaku* **43**, 443 (1975).
14. R. H. Condit, R. R. Hobbins, C. E. Birchenall, *Oxid. Met.* **8**, 409 (1974).
15. Following Kerridge *et al.* (17), we used the Fe-Ni-S phase diagram (in weight %) of R. W. Shewman and L. A. Clark, *Can. J. Earth Sci.* **7**, 67 (1970).
16. The composition of the P-rich inner layer is given in D. S. Lauretta, K. Lodders, B. Fegley Jr., *Meteorit. Planet. Sci.*, in preparation.
17. J. F. Kerridge, J. D. MacDougall, K. Marti, *Earth Planet. Sci. Lett.* **43**, 359 (1979).
18. E. Anders and N. Grevesse, *Geochim. Cosmochim. Acta* **53**, 197 (1989).
19. G. Dreibus, H. Palme, B. Spettel, J. Zipfel, H. Wänke, *Meteoritics* **30**, 439 (1995).
20. R. S. Lewis and E. Anders, *Proc. Natl. Acad. Sci. U.S.A.* **72**, 268 (1975).
21. N. P. Hanowski and A. J. Brearly, *Meteorit. Planet. Sci.* **31** (suppl.), A57 (1996).
22. B. Million, J. Ruzickova, J. Velisek, J. Vrestal, *Mater. Sci. Eng.* **50**, 43 (1981); D. C. Dean and J. I. Goldstein, *Metall. Trans. A* **17**, 1131 (1986).

23. This work was supported by NASA grant NAGW-3070. We thank the Field Museum in Chicago for providing the samples of Canyon Diablo, M. K. Crombie for helpful discussions, and D. T. Kremser for technical assistance. J. I. Goldstein and an anonymous referee provided constructive reviews.

4 February 1997; accepted 2 June 1997